Synaptic Mechanisms of Top-Down Control by The Auditory Cortico-Collicular Pathway

Hannah M. Oberle[1,2], Alex Ford[1], Jordyn Czarny[1], & Pierre F. Apostolides[1,3]*
1) Kresge Hearing Research Institute & Department of Otolaryngology, University of Michigan Medical School
2) Neuroscience Graduate Program, University of Michigan
3) Molecular and Integrative Physiology, University of Michigan Medical School
*corresponding author: piaposto@med.umich.edu

Abstract

Corticofugal projections to evolutionarily ancient, sub-cortical structures are ubiquitous across mammalian sensory systems. These “descending” pathways enable the neocortex to control ascending sensory representations in a predictive or feedback manner, but the underlying cellular mechanisms are poorly understood. Here we combine optogenetic approaches with *in vivo* and *in vitro* patch-clamp electrophysiology to study the projection from auditory cortex to the inferior colliculus (IC), a major descending auditory pathway that controls IC neuron feature selectivity, plasticity and auditory perceptual learning. Although individual auditory cortico-collicular synapses were generally weak, IC neurons often integrated inputs from multiple corticofugal axons that generated reliable, tonic depolarizations even during prolonged presynaptic activity. Latency measurements *in vivo* showed that descending signals reach the IC within 30 ms of sound onset, which in IC neurons corresponded to the peak of synaptic depolarizations evoked by short sounds. Activating ascending and descending pathways at latencies expected *in vivo* caused a NMDA receptor dependent, supra-linear EPSP summation, indicating that descending signals can non-linearly amplify IC neurons’ moment-to-moment acoustic responses. Our results shed light upon the synaptic bases of descending sensory control, and imply that heterosynaptic cooperativity contributes to the auditory cortico-collicular pathway’s role in plasticity and perceptual learning.

Introduction

The auditory system is organized as a network of feedback loops, such that most central auditory nuclei receive descending projections from higher levels of the processing hierarchy (Diamond et al., 1969; Saldaña et al., 1996; Winer et al., 1998, 2001; Doucet et al., 2003; Coomes and Schofield, 2004; Schofield et al., 2006; Suthakar and Ryugo, 2017). The auditory cortex is a major source of excitatory (glutamatergic) descending projections, with the density of descending fibers often rivaling that of ascending fiber tracts (Winer et al., 2001; Winer, 2006; Stebbings et al., 2014). These corticofugal projections likely play a major role in hearing by providing an anatomical substrate for "top-down" information to control early acoustic processing. Indeed, stimulating or silencing the auditory cortex *in vivo* changes spontaneous and sound-evoked activity throughout the central auditory system (Massopust and Ordy, 1962; Ryugo and Weinberger, 1976; Yan and Suga, 1998, 1999; Xiao and Suga, 2002; Yu et al., 2004; Nakamoto et al., 2008, 2010; Anderson and Malmierca, 2013; Kong et al., 2014; Vila et al., 2019; Blackwell et al., 2020; Qi et al., 2020), indicating that high-level activity regulates the moment-to-moment function of sub-cortical auditory circuits. However, little is known regarding the biophysical properties of auditory corticofugal synapses, nor do we understand how descending signals are integrated with ascending information. Given that synaptic dynamics and pathway integration are fundamental building blocks of neural circuit computations (Abbott et al., 1997; Zucker and Regehr, 2002; Stuart and Spruston, 2015), addressing these knowledge gaps is necessary to understand how the auditory cortex exerts control over early auditory processing.

Of particular interest is the descending projection from auditory cortex to the inferior colliculus (IC), a midbrain hub important for sound localization, speech perception, and an early site of divergence for primary and higher-order auditory pathways (Masterton et al., 1968; Krishna and Semple, 2000; Champoux et al., 2007; Sinex and Li, 2007; Joswig et al., 2015). The IC is generally sub-divided into a "lemniscal" central core and "non-lemniscal" dorsal and lateral shell regions whose neurons have distinct afferent and efferent connections (Faye-Lund and Osen, 1985; Loftus et al., 2008; Ayala et al., 2015; Chen et al., 2018). Whereas central IC neurons project mainly to the primary auditory thalamus (ventral medial geniculate nucleus; Mellott et al., 2014; Oliver, 1984), shell IC neurons preferentially project to secondary, higher-order auditory thalamic nuclei that subsequently funnel acoustic information to the amygdala and striatum (Oliver and Hall, 1978; LeDoux et al., 1990; Bordi and LeDoux, 1994; Mellott et al., 2014; Cai et al., 2019; Ponvert and Jaramillo, 2019). Auditory cortico-collicular axons terminate primarily in the shell IC, with comparatively fewer fibers in the central IC (Bajo et al., 2019; Chen et al., 2018; Lesicko et al., 2016; Song et al., 2018; Winer et al., 1998; Xiong et al., 2015; but see Saldaña et al., 1996). Thus, auditory cortico-collicular synapses seem uniquely positioned to modulate acoustic signals destined for limbic circuits supporting learned valence and habit formation; this prediction is further supported by the fact that chemical ablation of auditory cortico-collicular neurons selectively impairs certain forms of auditory perceptual learning while sparing the performance of previously learned task associations (Bajo et al., 2010). Nevertheless, little is known regarding how auditory cortico-collicular synapses control activity in single IC neurons. Intriguingly, auditory cortex inactivation typically does not abolish IC neuron sound responses, but rather causes divisive, non-monotonic changes in receptive field properties and feature selectivity (Yan and Suga, 1999; Nakamoto et al., 2008, 2010; Anderson and

Malmierca, 2013). Thus, descending transmission might operate in part via heterosynaptic interactions, perhaps by controlling how IC neurons respond to ascending acoustic inputs.

Here we employ electrophysiology and optogenetic approaches to identify how auditory cortico-collicular synapses transmit descending signals, and to understand how descending synapses control IC neuron responses to ascending inputs. We find that the majority of shell IC neurons receive monosynaptic inputs from auditory cortex and often integrate information from multiple distinct corticofugal axons. Synaptic latency measurements *in vivo* show that descending excitation reaches IC neurons ~5-7 ms after spike initiation in auditory cortex, such that cortical feedback will rapidly follow the onset of acoustically driven excitation. Somewhat surprisingly, NMDA receptors only modestly contribute to descending transmission. By contrast, excitatory intra-collicular synapses from the central IC, which are probably a major source of ascending acoustic signals to shell IC neurons, had a much larger NMDA component. Consequently, appropriately timed activity in ascending and descending pathways integrates supra-linearly owing to the cooperative activation of NMDA receptors. Our data reveal a key role for heterosynaptic non-linearities in the descending modulation of early acoustic processing. In addition, the results place important biophysical constraints on the synaptic learning rules that might support the auditory cortico-collicular pathway's role in experience-dependent plasticity and perceptual learning.

Results

Auditory cortico-collicular synapses robustly target superficial IC neurons

Corticofugal axons are predominantly restricted to the shell IC (Winer et al., 1998; Song et al., 2018), but little is known about the extent of functional synaptic connectivity between auditory cortex and IC neurons. We tested how auditory cortico-collicular synapses impact IC neurons by transducing the optogenetic activator Chronos in the auditory cortex of mice via intracranial AAV injections (Figure 1A), and 2-4 weeks later, performing *in vivo* whole-cell recordings from the ipsilateral IC of urethane anesthetized mice. GFP-tagged, Chronos expressing auditory cortico-collicular axons were primarily restricted to the ipsilateral dorsal-medial and lateral IC (Figure 1B), in agreement with previous studies. Single flashes of blue light from an optic fiber positioned over auditory cortex (1-5 ms duration; Figure 1C) reliably triggered excitatory postsynaptic potentials (EPSPs) in n = 21/38 IC neurons recorded from N = 8 mice (Figure 1D). EPSPs were primarily observed in superficial IC neurons, with the majority of unresponsive neurons located more ventrally, presumably in the central IC (Figure 1E; mean depth of cortico recipient and non-recipient neurons: 220 ± 23 vs. 354 ± 38 μm from surface, p=0.0036, Kolmogorov-Smirnov test). EPSPs had an onset latency of 10.3 ± 0.7 ms following light stimulation (Figure 1F), a peak amplitude of 3.5 ± 0.7 mV (Figure 1G), and a full-width at half-maximum of 18.4 ± 1.5 ms (Figure 1H). Interestingly, EPSP amplitudes varied over 2 orders of magnitude across different cells and were occasionally large enough to drive IC neurons beyond spike threshold (Supplemental Figure 1A). These data indicate that descending excitation can be quite potent, such that even brief and presumably sparse activity of auditory cortico-collicular neurons could in principle drive IC efferent signals independently of ascending inputs.

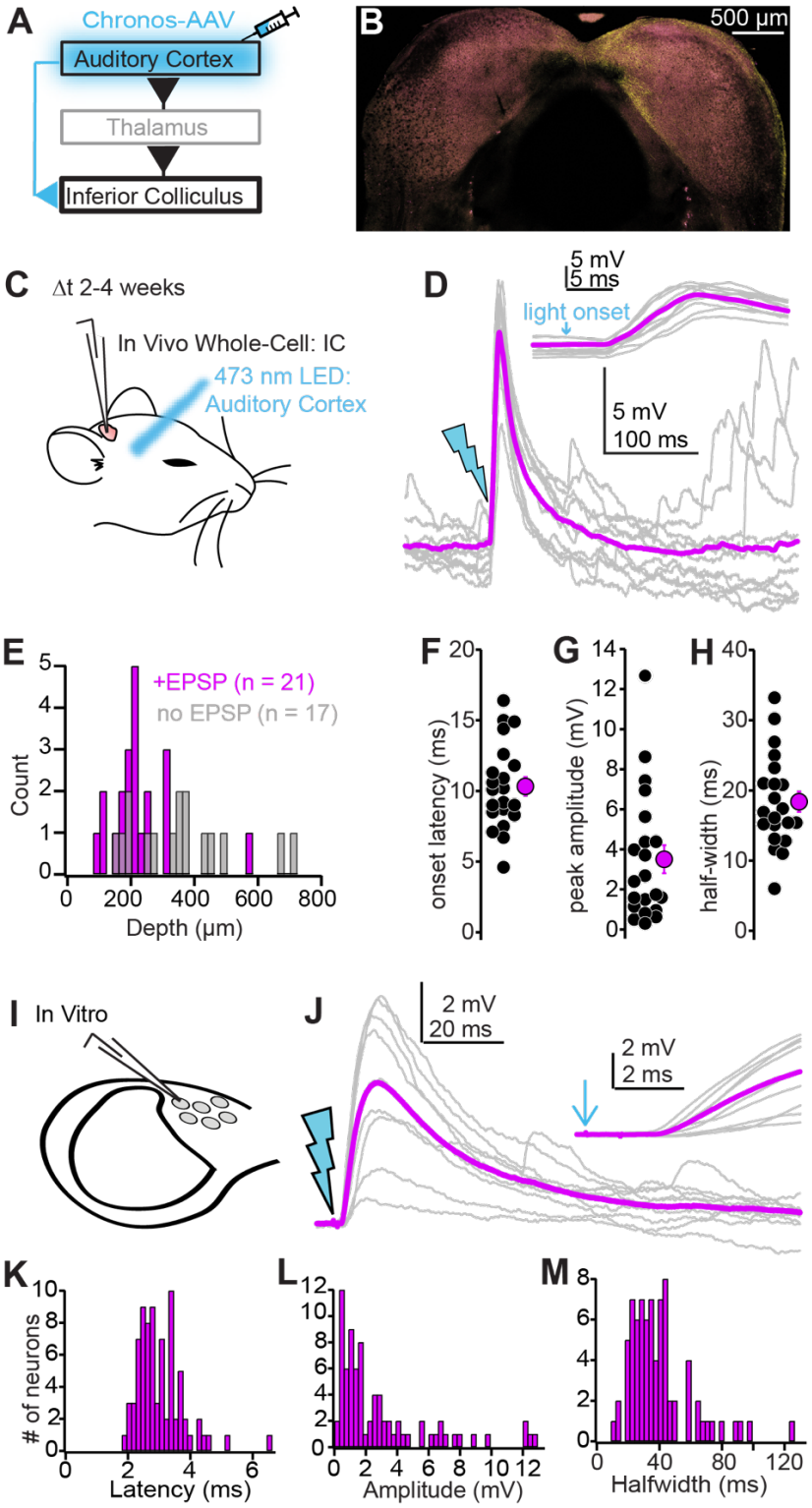

Figure 1: *Biophysical properties of auditory cortico-collicular synapses* **A)** Cartoon of experiment. **B)** Confocal stack of GFP-Chronos labeled axons mainly restricted to the shell IC. **C)** *In vivo* whole-cell recordings are obtained from IC neurons 2-4 weeks following Chronos injections; an optic fiber is positioned above the auditory cortex **D)** Example EPSPs following *in vivo* optogenetic stimulation. Gray traces are single trials; magenta is average. Inset is the EPSP rising phase at a faster timebase. **E)** Dorsal-ventral locations (relative to dura) for IC neurons where auditory cortical stimulation did (magenta) and did not (gray) evoke an EPSP. **F-H)** Summary of EPSP onset (F) amplitude (G), and half-width (H). **I)** whole-cell recordings obtained from dorso-medial shell IC neurons *in vitro*. **J)** EPSPs evoked by *in vitro* optogenetic stimulation (2 ms light flash). Inset: EPSP rising phase. **K-M)** Histograms of EPSP onset (K), amplitudes (L), and half-widths (M) *in vitro*.

Because the auditory cortex projects to many sub-cortical targets besides the IC, *in vivo* stimulation could drive polysynaptic excitation onto IC neurons that would complicate estimates of monosynaptic connectivity. We thus prepared acute IC brain slices from mice injected with Chronos in auditory cortex to quantify the functional properties of descending synapses in a more controlled setting. We targeted whole-cell current-clamp recordings specifically to neurons in the dorso-medial shell IC, as this region shows the highest density of corticofugal axons (Song et al., 2018; our Figure 1B). Stimulating auditory cortico-collicular axons via single blue light flashes delivered through the microscope objective (1-10 ms duration) drove EPSPs in n = 78 neurons from N = 40 mice (Figure 1I,J). EPSPs had short-latency onsets following photo-stimulation (Figure 1K; 3.0 ± 0.1 ms), indicating a monosynaptic rather than polysynaptic origin. EPSPs *in vitro* had a similar range and mean peak amplitude as those recorded *in vivo* (Figure 1L; 2.97 ± 0.35 mV, p=0.3, Mann-Whitney test), and similarly could drive spikes in a subset of recordings (Supplemental Figure 1B). Although the EPSP half-width was significantly slower *in vitro* compared to *in vivo* (Figure 1M; 39.6±2.3 ms, p<0.001, rank-sum test), this result is not surprising: The constant barrage of synaptic inputs *in vivo* is expected to generate a “high conductance state” that accelerates the membrane time constant (Destexhe et al., 2003).

In a separate set of experiments (n = 11 neurons from N = 6 mice), we quantified the kinetics of auditory cortical excitatory postsynaptic currents (EPSCs) as they appear at the soma using voltage-clamp recordings with a Cs^+ based internal solution (Supplemental Figure 2. Peak amplitude = 60.1 ± 14.4 pA; weighted decay time constant = 4.5 ± 0.5 ms; 10-90% rise time of 1.2 ± 0.2 ms). Altogether, our results show that auditory cortico-collicular synapses substantially depolarize shell IC neurons independent of network-level, polysynaptic activity. In addition, EPSP kinetics are such that descending excitation will undergo significant temporal summation at firing rates observed during sound-evoked activity of auditory cortico-collicular neurons (20-50 Hz; Williamson and Polley, 2019).

Synaptic strength reflects presynaptic convergence rather than unitary EPSP amplitudes

EPSP amplitudes spanned two orders of magnitude under our conditions (Figure 1G,L). Does this variability reflect a differential potency of individual synapses, or alternatively, differences in the number of presynaptic auditory cortical axons impinging onto individual shell IC neurons? We first estimated unitary EPSP amplitudes using a minimal stimulation paradigm designed to activate one (or very few) auditory cortico-collicular fibers. In these experiments, the LED intensity was titrated to the minimum power required for optogenetic responses to fluctuate between successful EPSPs and failures on a trial-by-trial basis (Figure 2A,B; mean failure rate across experiments: 44 ± 3%, n = 18 cells from N = 14 mice). The mean amplitude of successful EPSPs was generally small (0.84 ± 0.09 mV; Figure 2C) and similar to previous reports of unitary synapses between layer 5 pyramidal neurons in sensory cortex (Brown and Hestrin, 2009; Lefort et al., 2009). By contrast, progressively stronger LED flashes increased the amplitude of successful EPSPs compared to the minimal stimulation condition in many cells tested (n=15 cells from N = 11 mice; Figure 2D,E), indicating that multiple corticofugal axons can converge onto individual shell IC neurons. The ratio of maximum to minimum EPSP showing varied >10-fold across different experiments (median: 1.67, range: 0.91-24.04, Figure 2F), indicating that the EPSP amplitude variability across individual neurons likely reflects the number of presynaptic auditory cortical fibers recruited during stimulation

rather than differences in unitary strength. Importantly, the EPSP half-width was constant across the range of stimulus intensities (Figure 2D, inset. EPSP halfwidth ratios at maximal and minimal LED intensities: 1.04 ±0.07). This result indicates that increased LED intensities recruit more axons rather than prolonging Chronos activation and temporally dispersing vesicle release from single presynaptic boutons. We conclude that although the strength of individual auditory cortico-collicular synapses is weak, the convergence of multiple presynaptic fibers ensures that descending signals will substantially increase shell IC neuron excitability.

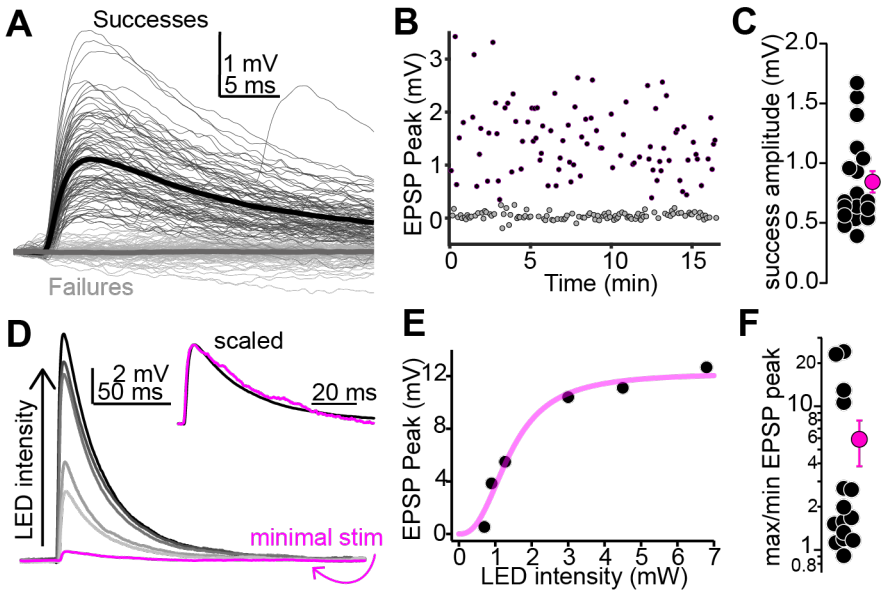

Figure 2: *Multiple auditory cortico-collicular fibers converge onto single shell IC neurons*. **A)** Example threshold optogenetic stimulation experiment. Thin black and gray traces are successes failures, respectively. Thick traces are averages. **B)** Diary plot from the experiment in panel A. black and gray symbols are successes and failures, respectively. **C)** Summary of putative unitary EPSP amplitudes **D)** Magenta: putative unitary EPSP (average of successes recorded at threshold stimulation). Black and Gray traces: averages of successes at increasing LED intensity. Data are from a different neuron as in A. Inset: Peak scaled and onset aligned EPSPs recorded at threshold and maximal intensity, revealing an identical time-course. **E)** EPSP peak amplitude is plotted as a function of LED intensity for the recording in (D). Magenta line is Hill fit. **F)** EPSP amplitude ratios at maximal and threshold LED intensities. Most values are >1, indicating convergence of at least 2 fibers. Of note, data are on a log scale.

Auditory cortico-collicular synapses contact shell IC neurons with diverse biophysical properties

IC neurons have a variety of firing patterns and membrane properties that potentially correspond to distinct neuronal subtypes (Smith, 1992; Li et al., 1998; Peruzzi et al., 2000; Sivaramakrishnan and Oliver, 2001; Ahuja and Wu, 2007; Sun and Wu, 2008; Moore and Trussell, 2017; Goyer et al., 2019; Naumov et al., 2019; Silveira et al., 2020). However, whether auditory cortico-collicular synapses contact biophysically homogenous or diverse neurons is unknown. We injected 300 ms positive and negative current steps to quantify spiking patterns and passive membrane properties in a subset of our *in vitro* experiments described above (n = 64 cells). 62/64 cortico-recipient shell IC neurons could be classified into one of four general categories. Over half of neurons (38/64) had significant spike rate adaptation during positive current injections (Figure 3A,B) and qualitatively similar firing patterns as the shell IC neurons recorded in rat slices by Smith (1992). However, 18 of these “adapting” neurons responded to negative current with a sustained hyperpolarization (Figure 3A), whereas 20 displayed a prominent I_h-like “sag” likely mediated by HCN channels (Figure 3B,

middle trace). These data suggest a minimum of two shell IC neuron sub-types with adapting firing patterns, which can be differentiated based on the extent of I_h sag. By contrast, other neurons had delayed first spikes (9/64, Figure 3C) or showed non-adapting discharge patterns (15/64, Figure 3D). Finally, 2/64 cells displayed a strikingly distinct phenotype, with a burst of spikes riding atop a "hump"-like depolarization similar to neurons expressing T-type Ca^{2+} channels (Figure 3E). EPSP amplitude and half-width of were similar across the four major categories (Peak amplitude: p=0.45; half-width: p=0.5, Kruskal-Wallis tests) despite marked differences in electrical properties. Thus, the auditory cortex broadcasts similarly strong signals to multiple, putatively distinct IC neurons, arguing that biophysical properties alone do not predict the strength of descending synapses.

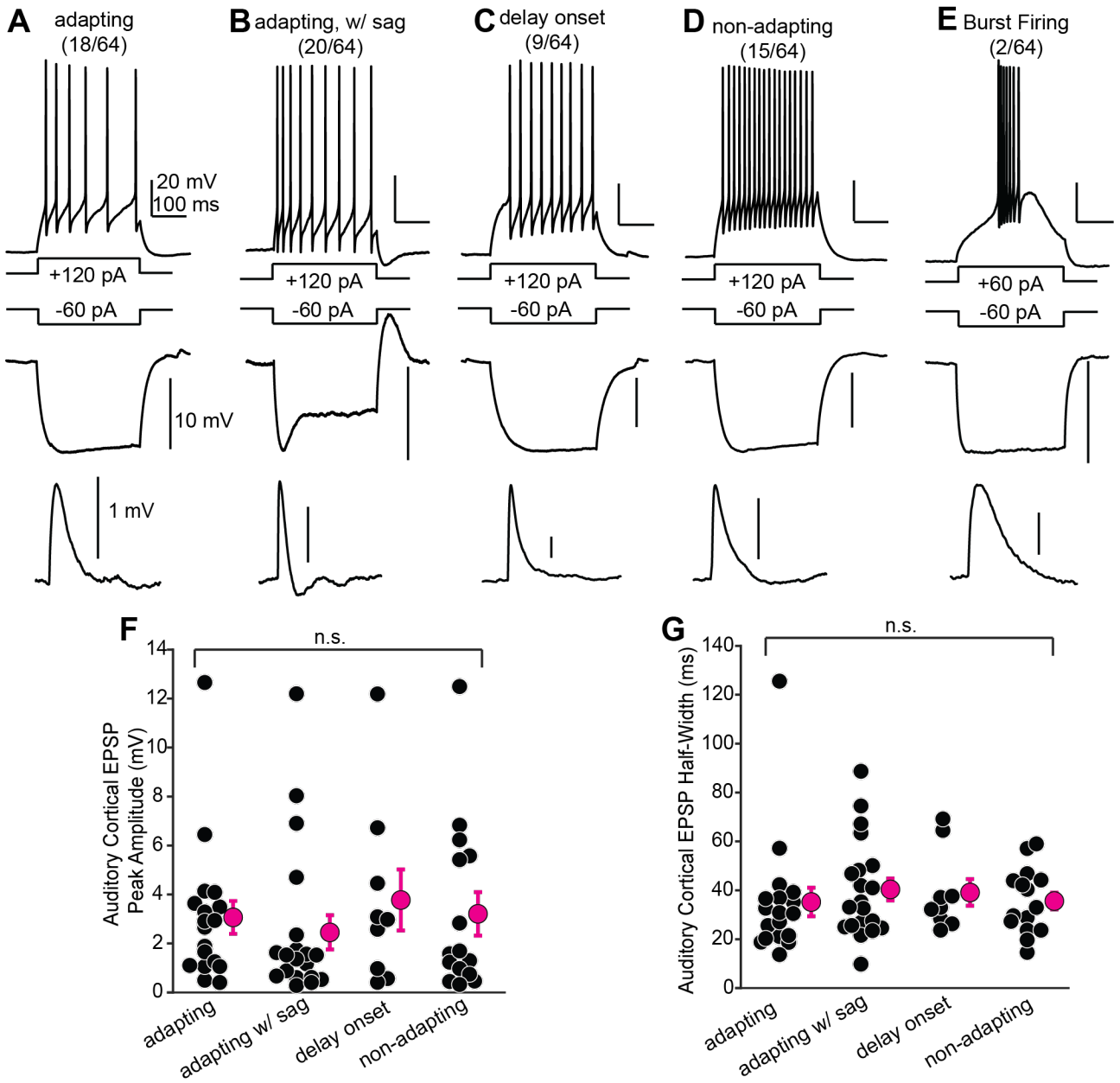

Figure 3: *Shell IC neurons receiving descending signals have diverse biophysical properties.* **A-E)** Examples of different shell IC neurons. Top and Middle traces are spike output and membrane hyperpolarization following positive and negative current steps, respectively. Lower traces: average auditory cortical EPSPs from the same neuron. **F, G)** EPSP peak amplitude (F) and half-width (G) as a function of biophysical category. Bursting neurons are omitted due to low n.

Temporal integration of auditory cortical inputs is moderately sub-linear

Auditory cortico-collicular neurons in awake mice respond to acoustic stimuli with ~10-50 Hz spike trains (Williamson and Polley, 2019). Given the kinetics of auditory cortico-collicular EPSPs (Figure 1), these spike rates are expected to result in significant temporal summation of descending signals. However, the use-dependent dynamics neurotransmitter release, as well as postsynaptic ion channels, can enforce sub- or supra-linear summation that effectively dictates the temporal integration of EPSPs (Markram et al., 1998; Pouille and Scanziani, 2004; Polsky et al., 2009). How do IC neurons integrate sustained cortical activity? We addressed this question by repetitively stimulating auditory cortico-collicular axons (10 light pulses at 20 or 50 Hz, 2 ms pulse width; Figure 4A,B, black traces; n = 12 neurons from N = 7 mice). We quantified temporal integration by comparing the peak EPSP amplitudes observed after each light flash in the train to the amplitudes expected from the linear summation of a single auditory cortico-collicular EPSP recorded in the same neuron (Figure 4A,B; magenta traces). The observed peak amplitude of the 10th EPSP in the train reached 92 ± 13 % and 77 ± 16% of that expected from linear summation at 20 and 50 Hz, respectively (Figure 4C,D). These results argue that at the population-level, auditory cortical firing rates are read out as moderately sub-linear shifts of the membrane potential towards threshold.

Auditory cortico-collicular neurons display elevated firing rates at ~20 Hz for the entirety of long-duration, complex sounds (e.g., 4 s long dynamic chord stimuli; Williamson and Polley, 2019). We thus wondered if descending synapses maintain transmission during sustained acoustic processing, or if synaptic depression instead limits descending signals to sound onset. Stimulating auditory cortical axons with 4 s trains of light pulses at 20 Hz (Figure 4E) drove fast EPSPs riding atop a steady-state, tonic depolarization (Figure 4F; mean amplitude of DC component during the final 1 s of stimulation: 1.18 ± 0.01 mV, p = 0.013, one-sample t-test compared to a hypothetical value of 0. n = 10 cells from n = 7 mice). Importantly, these effects were not an artifact of directly stimulating auditory cortico-collicular nerve terminals in brain slices: A similar tonic depolarization was observed in superficial IC neurons recorded *in vivo* using an optic fiber positioned over auditory cortex (Figure 4G,H; mean amplitude of DC component: 1.5 ± 0.7 mV, n=19 cells from n = 6 mice, p=0.53 compared to *in vitro* data, rank-sum test).

In addition, cessation of cortical stimulation *in vivo* also caused a long-lasting after-hyperpolarization (AHP) in 14/19 cells: The membrane potential rapidly fell below baseline after the last stimulus (τ = 76.5 ± 1.5 ms) and recovered over several seconds (τ = 2.6 ± 0.6 s; Supplemental Figure 3). Interestingly, this AHP was independent of postsynaptic spiking and thus may reflect buildup of feed-forward inhibition from local and long-range sources, or alternatively, a transient cessation of tonic descending excitation. Altogether, these experiments show that auditory cortico-collicular synapses can sustain transmission on seconds time scales via tonic and phasic excitation. In addition, the profound AHP following *in vivo* stimulation suggests that IC neuron excitability is bi-directionally yoked to auditory cortical firing patterns. Thus, increases as well as pauses in auditory cortico-collicular neuron activity may be of comparable significance to IC neurons.

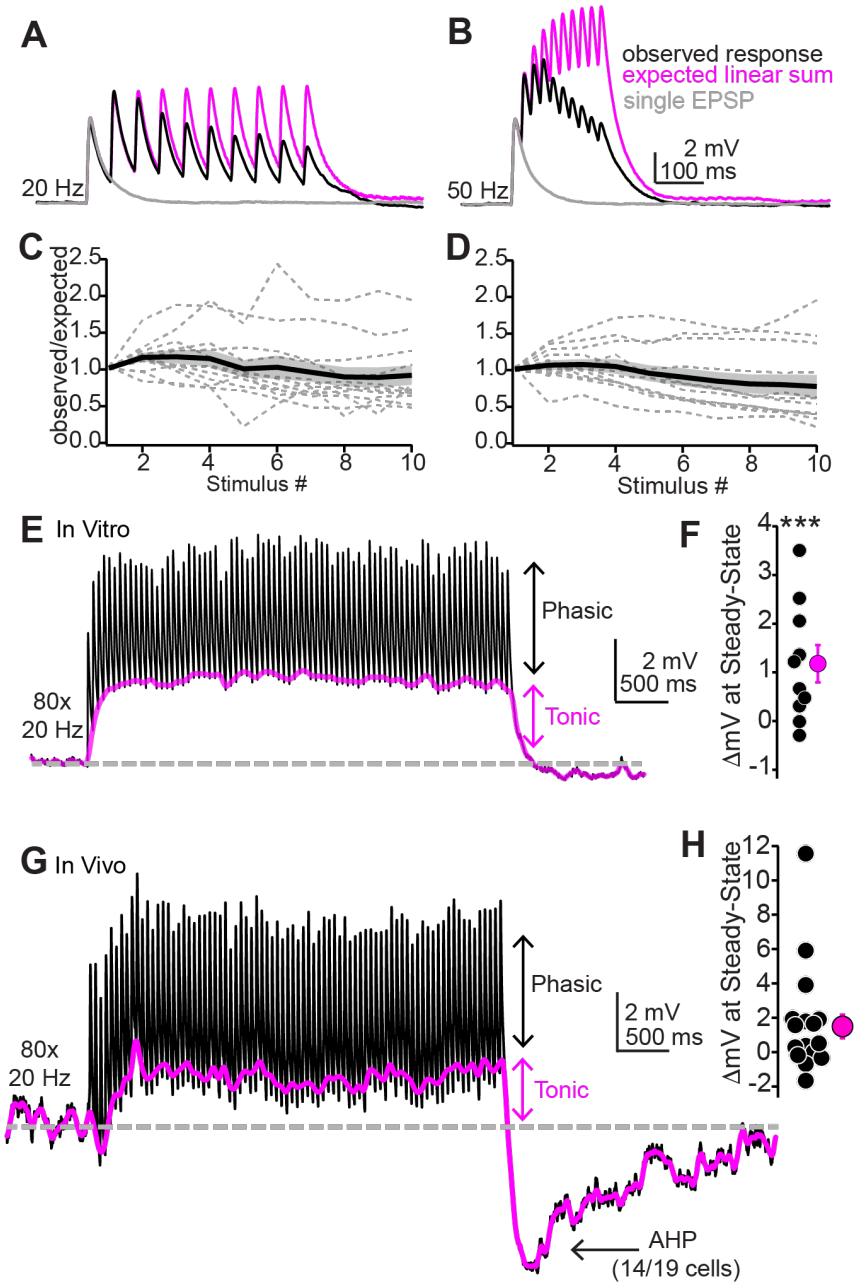

Figure 4: *Repetitive synaptic activity tonically depolarizes shell IC neurons despite sub-linear temporal summation of EPSPs.* **A,B)** Black traces: Average EPSPs evoked by 20 (A) or 50 Hz (B) trains of 10 light flashes. Gray: Average EPSPs evoked by a single 2 ms light flash recorded in the same neuron. Magenta: The expected response assuming linear summation of single EPSPs at each frequency. Of note is that the recorded EPSP amplitudes in the train are smaller than the expected linear sum. Data in A and B are from the same neuron. **C,D)** Summary of observed over expected amplitudes for EPSPs during 20 (C) or 50 Hz (D) trains. Gray dotted lines are individual neurons; black + shading are mean ± SEM **E)** Sustained auditory cortical transmission generates phasic EPSPs (black) riding atop a tonic depolarization (magenta) *in vitro*. **F)** Group data quantifying membrane potential changes at steady-state (final 1 s of stimulation). **G,H)** Same as E and F but during *in vivo* recordings. Of note is the large AHP.

NMDA receptors contribute to temporal integration of descending signals

Central excitatory transmission is predominantly mediated by AMPA and NMDA type glutamate receptors, with NMDA receptors being particularly crucial for dendritic integration (Larkum et al., 2009; Branco et al., 2010), associative plasticity (Kerchner and Nicoll, 2008), and learning (Morris et al., 1986). The auditory cortico-collicular pathway is involved in perceptual learning following monaural hearing loss (Bajo et al., 2010), and NMDA receptors in the avian IC shell homologue preferentially contribute to receptive fields generated by experience-dependent plasticity (Feldman et al., 1996). We thus asked to what extent auditory cortico-collicular synapses activate NMDA receptors in shell IC neurons. Interestingly, bath application of the AMPA/kainate receptor antagonist NBQX (10 µM) completely abolished EPSPs in all neurons tested (Figure 5A,B. Peak amplitude control: 1.93 ± 0.02 mV; NBQX: 0.09 ± 0.03 mV, p=0.004, n=9 cells from N = 7 mice, Wilcoxon sign-rank test), indicating that AMPA receptors mediate the overwhelming majority of synaptic charge at descending synapses.

By contrast, although the NMDA receptor antagonist R-CPP (5 µM) had minimal effect on the peak amplitude of auditory cortico-collicular EPSPs evoked with single light flashes (Figure 5C,D; n = 9 cells from N = 6 mice. Control: 3.3 ± 0.9 mV, R-CPP: 3.4 ± 0.9 mV, p = 0.67, paired t-test), R-CPP caused a modest but significant reduction in the EPSP half-width (Figure 5C,E; control: 35.7 ± 4.4 ms, R-CPP: 30.4 ± 4.7 ms. 17.6% reduction, p=0.016, paired t-test). In addition, depolarizing neurons to +30 to +40 mV in voltage-clamp (using a Cs^+-rich internal solution) slowed the weighted decay time constant of optogenetically evoked EPSCs by 8.2 fold compared to negative holding potentials (Supplemental Figure 4; -60 to -70 mV: 6.1 ± 0.9 ms, +30 to +40 mV: 50.0 ±0.8 ms, n = 5 cells from N = 3 mice), consistent with the biophysical properties of NMDA receptors. We conclude that although AMPA receptors mediate the bulk of descending transmission at resting membrane potentials, glutamate released from descending synapses nevertheless reaches synaptic NMDA receptors to shape EPSP kinetics. Thus, although NMDA receptors contribute little to the peak amplitude of EPSPs during sparse stimulation, they may nevertheless control the integration of repetitive activity across time.

Accordingly, R-CPP significantly reduced summation of auditory cortico-collicular EPSPs evoked by a train of 10 stimuli at 50 Hz (Figure 5F, G; n=10 cells from N = 8 mice. Main effect of drug condition in a two-way repeated measures ANOVA; $F(1,9)=5.91$, p=0.038), resulting in a 26% reduction in the cumulative integral of the synaptic depolarization (Figure 5F,H; control: 1.42 ± 0.35 mV * s, R-CPP: 1.03 ± 0.26 mV * s; p=0.012, paired t-test). These data show that NMDA receptors prolong the integration time window for descending signals, thereby boosting postsynaptic depolarizations during sustained cortical activity.

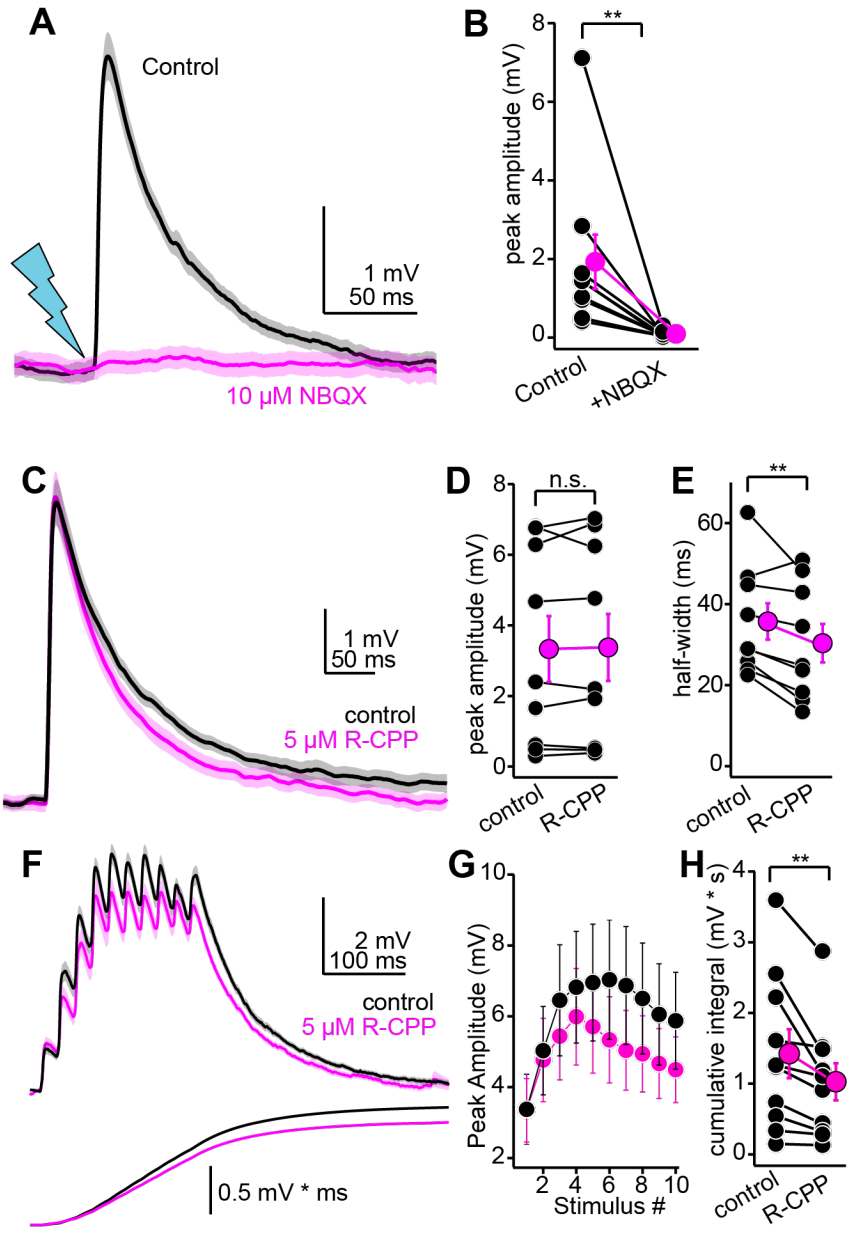

Figure 5. *Pharmacology of descending transmission.* **A)** EPSPs (mean ± SEM) from a single neuron before (black) and after (magenta) bath application of NBQX (10 μM). Of note is the absence of residual synaptic depolarization after NBQX. **B)** Summary data. For the effect of NBQX on descending EPSPs. **C)** EPSPs before and after R-CPP (black and magenta traces, respectively). **D, E)** Group data for the effect of R-CPP on EPSP peak amplitude (D) and half-width (E). Asterisks denote statistical significance. **F)** Upper panel: EPSPs (average ± SEM) evoked by 10 light flashes at 50 Hz. Black and magenta are in control and R-CPP. Lower panel is the cumulative integral of the waveforms. **G)** Group data showing amplitude of each EPSP in the train (mean ± SEM) before and after R-CPP (black and magenta, respectively). **H)** Group data for the effect of R-CPP on voltage integral as in F. Asterisks denote significance.

Differential contribution of NMDA receptors at ascending and descending synapses

The modest contribution of NMDA receptors at descending synapses is surprising, as previous studies suggest a rather prominent NMDA component at excitatory synapses in the IC (Smith, 1992; Wu, 2004; Kitagawa and Sakaba, 2019). We thus wondered if our results reflected a relative paucity of NMDA receptors at all excitatory synapses onto shell IC neurons, or rather a unique feature of auditory cortico-collicular synapses. Shell IC neurons receive a prominent intra-collicular projection from the central IC which likely transmits a significant amount of ascending acoustic information (Saldaña and Merchán, 1992; Saldaña et al., 1996; Sun and Wu, 2009). We tested if the NMDA component differed between ascending and descending EPSPs in the same neuron using a dual pathway stimulation approach *in vitro*: A bipolar stimulating electrode was positioned in the central IC and Chronos was expressed in auditory cortex to activate ascending and descending synapses, respectively (Figure 6A). 2.5-5 µM gabazine was present in all experiments to isolate excitatory transmission. Repetitive stimulation of either pathway (5x, 50 Hz) led to summating EPSPs which were differentially sensitive to NMDA receptor blockade (Figure 6B-C): 5 µM R-CPP reduced the cumulative integral of central IC and auditory cortical EPSPs to 44±4% and 78±4% of baseline, respectively (Figure 6D, n=9 cells from n = 8 mice, p=0.0004, paired t-test), indicating that NMDA receptors contributed less at descending compared to ascending synapses. Thus, the extent of NMDA receptor contribution to descending transmission reflects a synapse-specific property of auditory cortico-collicular inputs rather than the global distribution of NMDARs in shell IC neurons.

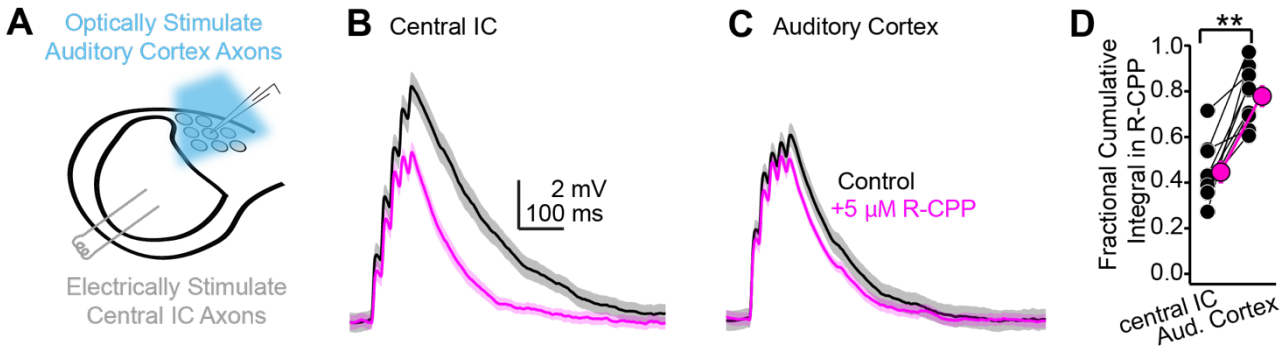

Figure 6. *Differential contribution of NMDA receptors at ascending and descending synapses.* **A)** Cartoon of experiment: Blue light flashes delivered through the microscope objective activate descending auditory cortico-collicular axons; a bipolar electrode in the central IC stimulates ascending central ->shell IC axons. **B,C)** EPSPs evoked by 5x 50 Hz stimulation of central IC (B) or auditory cortex (C) axons, in absence or presence of R-CPP (black and magenta, respectively). Data in panels B and C are from the same neuron. **D)** Group data quantifying the fractional EPSP remaining in R-CPP (as measured by the cumulative integral of the EPSP waveform) for central IC and auditory cortico-collicular synapses.

Auditory cortical inputs are predicted to arrive at the peak of EPSPs evoked by transient sounds

Layer 5 auditory cortico-collicular neurons in awake mice respond to sound with a mean first-spike latency of ~21 ms (Williamson and Polley, 2019). This value is surprisingly shorter than reported first spike latencies in shell IC neurons (~35 ms; Lumani and Zhang, 2010). Whether auditory cortical excitation arrives before, during, or after the onset of sound-evoked EPSPs in shell IC neurons effectively determines how ascending and descending signals integrate at the single cell

level, but the relative timing of distinct inputs onto IC neurons is unknown. We thus quantified the relative timing of ascending sound-evoked and descending cortical EPSPs using *in vivo* whole-cell recordings from superficial IC neurons of anesthetized mice. We first determined the onset latency of descending EPSPs in IC neurons using electrical stimulation of the auditory cortex (Figure 7A). We employed electrical, rather than optogenetic stimulation for these experiments because spike onset following optogenetic stimulation is limited by the cell's membrane time constant and effective spike threshold, whereas electrical stimulation bypasses somato-dendritic depolarization by directly triggering axonal spikes. Single shocks delivered to the auditory cortex evoked EPSPs with an onset latency of 5.4 ± 0.6 ms (n = 7 cells from n = 4 mice; mean depth of recorded neurons 188 ± 14 µm, Figure 7B,C), indicating that descending information reaches IC neurons within a few ms of AP initiation in auditory cortex. Since the mean first-spike latency of auditory cortico-collicular neurons is ~21 ms (Williamson & Polley, 2019) and the synaptic latency is 5-8 ms (Figure 7B,C), these data collectively argue that that cortical feedback begins to excite IC neurons <30 ms after sound onset. Furthermore, assuming an axon path length of ~8 mm from auditory cortex to shell IC (Llano et al., 2014) and a synaptic release delay of ~2 ms, the data suggest a minimum conduction velocity of ~2.35 m/s. These values are similar to conduction velocity estimates for the myelinated axons of layer 5 pyramidal neurons in rodents (2.9 m/s; Kole et al., 2007), suggesting that layer 5, and not unmyelinated layer 6 neurons, are the dominant source of descending signals to the IC.

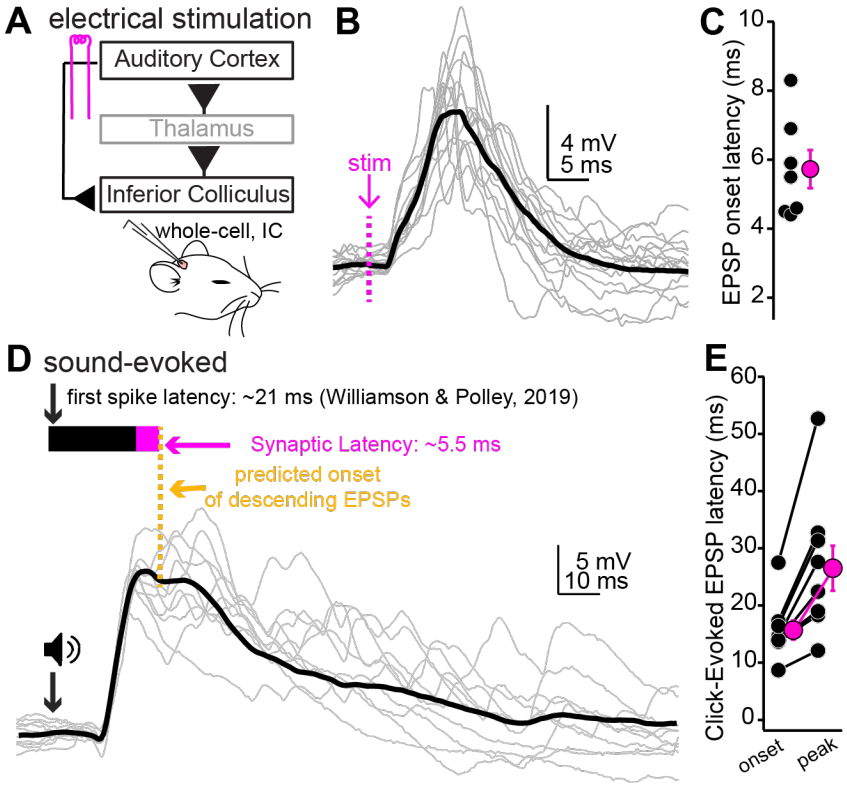

Figure 7: *Auditory Cortical feedback is predicted to collide with the peak of ascending excitation.* **A**) Cartoon of experiment. **B)** Example recording showing short latency EPSPs following a single shock to the auditory cortex. Dotted line is onset of stimulation. Gray traces are single trials; black is average. The stimulation artifact, as well as APs riding atop the cortical EPSP, were blanked for clarity. **C)** Group data for EPSP onset latency. **D)** EPSPs evoked by a 200 µs click. Arrow and speaker show sound onset. Data are from a different neuron than in B. Black and magenta bars above the traces show the reported first spike latency of auditory cortico-collicular neurons from previous work and the synaptic latency calculated from panels B and C, respectively. **E)** Group data for onset and peak latency of click-evoked EPSPs.

We next calculated the timing of sound-evoked excitation onto superficial IC neurons using broadband "click" transients (Figure 7D, n = 10 cells from N = 7 mice. Mean depth: 204±23 µm). Although sound-evoked EPSPs were typically sub-threshold under our conditions, click stimuli occasionally drove spikes in 5/10 experiments (33.8 ± 16.6% of trials), with mean first spike latencies of 29.4±7.6 ms, similar to previous reports (Lumani and Zhang, 2010; Geis et al., 2011). Sound evoked EPSPs had mean onset and peak latencies of 15.7 ± 1.7 and 26.5 ± 3.9 ms, respectively (Figure 7E), indicating that cortical feedback lags the rising phase of sound-evoked excitation by a mere 10-15 ms. Importantly, the data further suggest that cortical excitation will arrive prior to, or in very close succession with, the peak of EPSPs evoked by transient sounds, such that cortical feedback could in principle dictate the first spike latencies of shell IC neurons.

NMDA receptor dependent, supra-linear pathway integration in shell IC neurons

Our latency measurements (Figure 7) suggest that ascending information is rapidly followed by descending cortical excitation. This temporal overlap is intriguing because ascending and descending synapses express NMDA receptors (Figure 6), which in other cell-types, enable cooperative interactions between co-active pathways onto the same neuron (Takahashi and Magee, 2009; Harnett et al., 2012). We thus hypothesized that appropriately timed cortical feedback might integrate non-linearly with ascending inputs from the central IC, thereby generating a synaptic depolarization larger than expected from the sum of either pathway active in isolation. We tested this idea *in vitro* using our dual pathway stimulation approach (Figure 6) while recording from shell IC neurons. We first recorded the synaptic depolarization following stimulation of ascending and descending pathways in isolation (5 stimuli at 50 Hz; Figure 8A, upper traces).

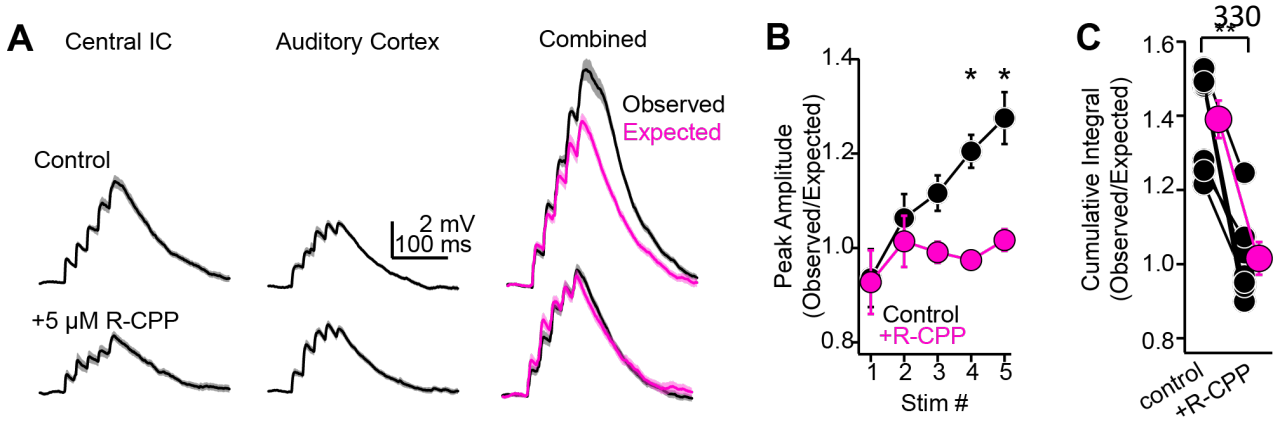

Figure 8: *NMDA-receptor dependent, supralinear pathway integration.* **A)** Upper and lower traces are during baseline conditions and after bath applying R-CPP. Left and middle panels: EPSPs during electrical or optogenetic stimulation of central IC or auditory cortical axons, respectively (5x, 50 Hz stimuli). Right panel ("Combined"): Black traces are the observed depolarization during simultaneous stimulation of both pathways. Magenta is the depolarization expected from the arithmetic sum of the waveforms following stimulation of either pathway alone (e.g., left and middle traces). Of note, the observed depolarization under control conditions is larger than expected from linear summation; blocking NMDA receptors linearizes pathway integration (compare black and magenta traces in R-CPP). **B)** Group data plotting the ratio of observed and expected peak amplitude for each of 5 EPSPs in a 50 Hz train during synchronous activation of central IC and auditory cortical synapses. Asterisks denote statistical significance of Bonferroni post-hoc test for the fourth and fifth stimuli following a main effect of drug condition (p=0.038, F(1,9), Two-way repeated measures ANOVA). **C)** Group data, observed over expected ratio of the cumulative integral during combined pathway activation in control conditions and in the presence of R-CPP. Asterisks denote statistical significance (sign-rank test).

We next simultaneously activated the two pathways such that the onset of cortical EPSPs collided with the peak of ascending EPSPs, as predicted from our *in vivo* latency measurements (Figure 7). The observed depolarization during synchronous pathway activation was on average significantly larger than expected from the arithmetic sum of each pathway stimulated alone (Figure 8A; n=12 cells from N=9 mice. Cumulative integral observed: 1.90 ± 0.35 mV*ms, expected: 1.45±0.22 mV*ms, p=0.007, paired t-test test), indicating that coincident activity of ascending and descending pathways summates supra-linearly. Importantly, R-CPP mostly abolished this supra-linear summation, such that the depolarization during coincident activation in R-CPP now equaled the expected sum of each pathway activated alone (Figure 8B,C, lower traces; n=7 cells from N = 7 mice. Observed/Expected control: 1.39±0.05; in R-CPP: 1.02±0.04, p=0.0156, sign-rank test). Thus, synaptic NMDA receptors provide a supra-linear boost when descending excitation follows ascending activity, thereby promoting the non-linear mixing of distinct pathways in single IC neurons.

Discussion

We have shown that the majority of neurons in the superficial (shell) IC layers receive reasonably strong excitation from auditory cortex that is predicted to arrive ~30 ms following sound onset. These synaptic properties could enable a context-dependent modulation of IC neurons across multiple timescales. Indeed, the rapid onset of descending EPSPs following cortical spikes (~5-8 ms) is more than twice as fast as sensory-evoked cortical gamma rhythms (30-50 Hz). Thus, descending signals could effectively synchronize neural ensembles across the ascending auditory hierarchy either to the temporal envelope of sound (Weible et al., 2020) or to internally generated rhythms. Furthermore, descending synapses sustained transmission and drove tonic depolarizations even during seconds-long activity patterns, such that IC neurons may also integrate slower cortical state fluctuations. Intriguingly, auditory cortical neurons in behaving animals show enhanced firing rates during the delay period of auditory working memory tasks (Gottlieb et al., 1989) which apparently, precedes similar activity patterns in prefrontal cortex (Huang et al., 2016). If these working memory related neuronal ensembles include auditory cortico-collicular neurons, sustained transmission from descending synapses could cause seconds-long increases in IC neuron excitability based on working memory content. Accordingly, persistent delay period activity is observed in ~10% of IC neurons when rats engaged in an auditory working memory task (Sakurai, 1990), although future studies are necessary to determine the extent to which this activity is inherited from descending auditory cortical pathways.

Finally, although our data suggest that shell IC neurons are the major target of descending fibers, the non-uniform thickness of the IC shell across medial-lateral axis (Barnstedt et al., 2015) indicates we cannot rule out that some of our *in vivo* data are from neurons in the most dorsal region of the central IC. Indeed, *in vivo* intracellular recordings from neurons in the deep IC layers report EPSPs following auditory cortex stimulation (Mitani et al., 1983; Qi et al., 2020), implying that some functional cortical synapses may in fact target central IC neurons. However, *in vitro* circuit mapping experiments imply that monosynaptic connections between auditory cortex and central IC

are likely very rare (Xiong et al., 2015; Song et al., 2018), such that shell IC neurons likely process the bulk of descending signals.

Synapse-specific contribution of NMDA receptors in shell IC neurons

The minor contribution of NMDA receptors to auditory cortico-collicular transmission is somewhat surprising, as synaptic NMDA receptors are activated even at hyperpolarized membrane potentials in central IC neurons (Ma et al., 2002; Wu, 2004; Goyer et al., 2019; Kitagawa and Sakaba, 2019). However, our results do not simply reflect a global paucity of NMDA receptors at excitatory synapses onto dorso-medial shell IC neurons, but rather can be explained by a pathway specific contribution of specific glutamate receptor sub-types to the synaptic depolarization: NMDA receptor blockade reduced EPSPs to a greater extent at central IC -> shell IC compared to auditory cortico-collicular synapses. Although a simple explanation is that the total number of synaptic NMDA receptors in shell IC neurons differs in a pathway specific manner, we cannot exclude differences in NMDA receptor subunit composition (Schwartz et al., 2012), glutamate diffusion (Arnth-Jensen et al., 2002), and synapse location (Branco et al., 2010; Song et al., 2018) as contributing factors.

Non-linear integration of ascending and descending signals

Intra-collicular synapses originating from the central IC likely provide a significant amount of ascending acoustic input to shell IC neurons. Indeed, reported first spikes latencies of central IC neurons typically lead the onset of sound evoked EPSPs in shell IC neurons (Syka et al., 2000; Hurley and Pollak, 2005), and central IC neurons send tonotopically organized axonal projections to the IC shell that conspicuously mirror the tonotopic distribution of best frequencies in the shell IC (Saldaña and Merchán, 1992; Wong and Borst, 2019). By contrast, the onset of sound-evoked EPSPs in shell IC neurons typically begin prior to the reported first spikes of auditory cortico-collicular neurons, thereby ruling out the possibility that acoustic responses are solely inherited from auditory cortex. Instead, axonal conduction velocities along ascending and descending pathways impose an obligatory delay such that cortical feedback excitation arrives ~25-30 ms following the onset of sound-evoked EPSPs. Notably, while glutamate released from ascending terminals will have unbound and diffused away from low-affinity synaptic AMPA receptors prior to the onset of cortical feedback excitation (Clements et al., 1992), high-affinity NMDA receptors are expected to remain bound with glutamate during this time (Lester and Jahr, 1992). Extracellular Mg^{2+} imparts a voltage-dependence to the NMDA receptor channel; the additional depolarization provided by cortical feedback would thus be expected to cooperatively enhance current flowing through NMDA receptors at ascending synapses active immediately prior to the onset of cortical feedback. This prediction is supported by our data showing a NMDA receptor-dependent, supra-linear summation of ascending and descending inputs that are activated similar to their expected timing *in vivo*. These single-cell, biophysical operations can potentially explain the non-linear changes in IC neuron receptive fields during cortical inactivation (Yan and Suga, 1999; Nakamoto et al., 2008, 2010).

NMDA receptor dependent non-linearities are typically thought of as unique features of cortical pyramidal neurons that support to the computational power of these high-level microcircuits. Nevertheless, multiplicative integration of sound localization cues has been observed in single neurons of barn owl IC (Peña and Konishi, 2001; 2002), and the NMDA receptor dependent non-

linearity we observe is comparable in magnitude to that reported during clustered activation of neighboring synapses in CA1 neurons (Harnett et al., 2012). Together, these data suggest that cooperative interactions between temporally correlated inputs may be a common neuronal operation throughout the central nervous system. An important distinction however is that most, if not all excitatory synapses in pyramidal neurons reside on dendritic spines; this compartmentalization greatly limits any cooperative interactions to neighboring synaptic inputs on the same branch (Gasparini and Magee, 2006; Losonczy and Magee, 2006). By contrast, auditory cortico-collicular axons often form large (~5 μm^3) synapses on the soma of dorsal IC neurons (Song et al., 2018). Depending on the impedance mismatch between the somatic and dendritic compartments, synaptic depolarizations at the soma could propagate passively throughout the neuron's multiple dendrites, thereby enabling cortical signals to non-linearly control ascending information irrespective of the spatial relationship of co-active inputs. However, further studies are necessary to identify the precise anatomical relationship between ascending and descending synapses in single IC neurons.

Implications for experience-dependent plasticity and perceptual learning

Several studies now show that layer 5 corticofugal pyramidal neurons are necessary for perceptual learning in multiple different sensory tasks. Optogenetic inhibition of layer 5 pyramidal neurons in somatosensory cortex prevents behavioral adaptation following cue-related changes in a tactile detection task, although the same manipulation had no effect on touch perception (Ranganathan et al., 2018). Similarly, lesioning visual corticostriatal neurons prevents acquisition, but not performance of a visual detection task (Ruediger and Scanziani, 2020). In the auditory system, chemical lesions of auditory cortico-collicular neurons prevent the experience-dependent recovery of sound localization following monaural hearing loss (Bajo et al., 2010), although auditory cortex becomes dispensable for sound-localization once animals have learned to localize sounds using monaural cues (Bajo et al., 2019). Thus, although necessary for perceptual learning, corticofugal synapses may not be the primary locus of experience-dependent plasticity. Indeed, classic studies in barn owls suggest that ascending central IC -> external (shell) IC synapses are the first site of experience-dependent, spatial map plasticity in the auditory system (Brainard and Knudsen, 1993). In tandem with our current study, these results suggest that auditory cortico-collicular synapses' contributions to perceptual learning may not lie in their explicit ability to undergo classical Hebbian associative plasticity, but rather as permissive forces of heterosynaptic plasticity at ascending synapses.

Methods

Surgery for viral injections: All experiments were approved by the University of Michigan's IACUC and performed in accordance with NIH's Guide for the care and use of laboratory animals. All surgical procedures were performed under aseptic conditions. Surgeries were performed on 4-7 week old male or female C57BL6/J mice purchased from Jackson Labs or offspring of CBA x C57BL6/J matings bred in house. Mice were deeply anesthetized with 4-5% isoflurane vaporized in O_2 and mounted in a rotating stereotaxic frame (model 1430, David Kopf Instruments). Isoflurane was subsequently lowered to 1-2% to maintain a deep anesthetic plane, as assessed by the

absence of paw withdrawal reflex and stable respiration (1-1.5 breaths/s). Body temperature was maintained near 37-38° C using a feedback controlled, homeothermic heating blanket (Harvard Apparatus). Mice were administered 5 mg/kg carprofen after induction as a pre-surgical analgesic. The scalp was clear of hair, swabbed with betadine, and a small incision was made in the skin overlying the left hemisphere. Topical 2% lidocaine was then applied to the wound margins. The stereotaxic frame was rotated ~50 degrees, allowing a vertical approach perpendicular to the layers of auditory cortex. A 200-400 µm craniotomy was carefully opened over the left auditory cortex (-2.75 mm from Bregma, centered on the lateral ridge) using a 0.5 mm diameter dental burr (19007-05, Fine Science Tools) and Foredom microdrill. The skull was frequently irrigated with chilled phosphate buffered saline (PBS) to prevent overheating during drilling. Following the craniotomy, a glass pipette (0.1-0.2 mm diameter at the tip) containing the pAAV-Syn-Chronos-GFP virus (Addgene #59170-AAV1) penetrated the auditory cortex at a rate of <10 µm/s using a motorized micromanipulator. A total of 100-200 nL virus was injected at 2-4 sites 810 and 710 µm below the pial surface (25-50 nL per site). Following injections, the pipette was maintained in place for an additional 5 min before slowly retracting at a rate of <10 µm/s. At the end of the surgery, the craniotomy was filled with bone wax, the skin was sutured, and the mouse was removed from the stereotax. Immediately following surgery, mice were given an analgesic injection of buprenorphine (0.03 mg/kg, s.c.) and allowed to recover on a heating pad before returning to their home cage. An additional post-operative dose of carprofen was administered 24 hours following surgery.

In vivo electrophysiology: 2-4 weeks following viral injections, mice were deeply anesthetized with isoflurane and mounted in a stereotax as described above. The skin overlying the skull was removed, the left temporal muscle was retracted, the stereotax was rotated ~50 degrees, and a 2-2.5 mm craniotomy was carefully opened over the left auditory cortex. For optogenetic stimulation in Figure 1, the dura overlying the auditory cortex was left intact and a cranial window was implanted over the exposed brain with cyanoacrylate glue and dental cement. For the electrical stimulation experiments in Figure 7, a small slit was carefully made in the dura and the craniotomy was subsequently sealed with silicone elastomer. The stereotaxic frame was returned to the horizontal position and a custom titanium headbar was affixed to the skull with dental cement. A 300-500 µm craniotomy was opened over the left IC and filled with a silicone elastomer plug. The mouse was then removed from the stereotax, anesthetized with urethane (1.5 g/kg, i.p.), and head-fixed in a custom-made sound attenuation chamber. Body temperature during the experiment was maintained at 37-38° C with a custom designed, feedback-controlled heating blanket. For optogenetic stimulation, a 0.5 NA, 400 µm core optic fiber (Thorlabs M45L02) coupled to a 470 nm LED (Thorlabs M470F3) was mounted on a micromanipulator and positioned <1 mm away from the auditory cortex cranial window. For electrical stimulation experiments, the silicone plug over auditory cortex was removed and a bipolar platinum-iridium electrode (FHC 30210) was carefully inserted ~800 µm into auditory cortex at an angle roughly perpendicular to the cortical layers. Electrical stimuli were delivered via a custom stimulus isolator designed in house. Sound clicks (0.2 ms duration) were presented at ~91 dB peak equivalent SPL via a free-field speaker (Peerless XT25SC90-04) positioned ~10 cm from the mouse's right ear. For whole-cell recordings, the silicone plug over the IC was removed and patch-clamp recordings were obtained from IC neurons via the "blind patch" approach using pipettes filled with K^+-rich internal solution containing (in mM): 115 K-Gluconate, 4 KCl, 0.1 EGTA, 10 HEPES, 14 Tris-Phosphocreatine, 4 Mg-ATP, 0.5 Tris-GTP,

4 NaCl, pH 7.2-7.3, 290 mOsm (open tip resistance: 5-10 MΩ). Data were acquired using an AM Systems model 2400 patch-clamp amplifier, online filtered at 2-10 kHz, and digitized at 50 kHz with a National Instruments PCI-6343 card + BNC2090A interface controlled by Matlab based acquisition software (Wavesurfer). Data were recorded with the amplifier's pipette capacitance neutralization circuitry activated. Series resistance was typically between 20-60 MΩ.

In vitro electrophysiology: 2-4 weeks following viral injections, mice were deeply anesthetized with isoflurane, swiftly decapitated, and the brains carefully removed in warm (~34° C), oxygenated ACSF containing (in mM): 119 NaCl, 25 $NaHCO_3$, 3 KCl, 1.25 NaH_2PO_4, 15 glucose, 1 $MgCl_2$, 1.3 $CaCl_2$, 1 ascorbate, 3 pyruvate. 200-300 µm thick coronal slices of the IC were prepared with a vibratome (Campden Instruments). On each slice, a small cut was made in the lateral portion of the right cerebellum or right IC to aid with visual identification of the un-injected hemisphere. Slices were then incubated at 34° C in a holding chamber filled ACSF for 25-30 min and subsequently stored at room temperature. Experiments were generally performed within 3-4 hours following slice preparation. Following incubation, a slice was transferred to a recording chamber and held in place with single strands of unwaxed dental floss tightly strung around a platinum "harp". The slice was continuously perfused with oxygenated ACSF heated to 32-34° C (2-4 mL/min; chamber volume: ~ 1 mL). 2-5 µM SR95531 was added to the ACSF to block $GABA_A$ receptors in experiments of Figure 5C-H, Figure 6, Figure 8, Supplemental Figures 2 and 4, and some experiments of Figure 1. Neurons in the dorso-medial shell IC were visualized via DIC or Dodt contrast optics using a 40x or 63x objective (Zeiss Axioskop 2 FS Plus or Olympus BXW51 microscope). Neurons were targeted for whole-cell current-clamp recordings with pipettes filled with the same K^+-rich internal solution used for *in vivo* recordings (open tip resistance: 3-6 MΩ). For whole-cell voltage clamp experiments, the internal solution contained (in mM): 110 Cesium Methanesulfonate, 10 QX-314-Bromide, 0.1 EGTA, 10 HEPES, 0.5 Tris-GTP, 4.5 MgATP, 5 TEA-Cl, 10 Tris-phosphocreatine. In some experiments, 30 µM Alexa 594 or 0.1% biocytin were added to the internal solution to visualize neuronal morphology via online fluorescence or post-hoc histological reconstruction.

Data were acquired with a Multiclamp 700B or AM System model 2400 amplifier, online filtered at 2-10 kHz, and digitized at 50 kHz with a National Instruments PCI-6343 card + BNC2090A interface controlled by Wavesurfer. In current clamp, pipette capacitance neutralization was employed and bridge balance was maintained (series resistance typically 10-30 MΩ). In a few instances, a small amount of negative bias current (-5 to -50 pA) was injected to hyperpolarize neurons and prevent spike initiation during optogenetic activation of cortico-collicular synapses. Series resistance compensation was employed in voltage clamp experiments (60-80%, bandwidth: 3 kHz). For dual pathway experiments, the central IC was electrically stimulated using an AM systems model 2100 stimulus isolator delivering biphasic shocks to a theta glass bipolar electrode placed ~500 µm from the recorded neuron. Drugs were obtained from Tocris or HelloBio, aliquoted as stock solutions in distilled water, and stored at -20 C until the day of the experiment.

Data analysis: Electrophysiology data were analyzed using custom Matlab scripts. EPSP analyses were performed on averages of multiple trials (typically >10 trials per condition) after baseline membrane potential subtraction and lowpass filtering at 1 kHz unless explicitly noted in the text. Peak amplitudes of single EPSPs were calculated by averaging data points ±0.1 ms around the

local maximum following optogenetic stimulation Halfwidths are calculated as the full width at half-maximum of the peak. EPSP onset latency was defined as the time following optogenetic stimulus onset when the membrane potential reaches 20% of peak. The tonic EPSP amplitude during 20 Hz trains was calculated as follows: We first linearly interpolated the membrane potential data between each light flash to remove the phasic EPSP component. The trace was then smoothed using a 50 ms sliding window. Datapoints during the final 1s period of the stimulus train were then averaged to estimate the amplitude of tonic membrane potential change. In certain experiments of Figures 4, 7, and 8, train stimuli and click sounds occasionally triggered APs in IC neurons both *in vivo* and *in vitro*. In these cases, APs were digitally removed prior to averaging the traces by linearly interpolating 0.1-0.2 ms of datapoints after the membrane potential crossed spike threshold (~20 mV/ms). Shock artifacts during electrical stimulation experiments were similarly removed via linear interpolation. In summary plots, black symbols are individual cells, magenta is mean ± SEM, and lines connect data from the same recording unless otherwise stated.

The expected linear waveforms for temporal summation experiments were calculated as follows. The average waveform of a single optogenetically evoked EPSP was peak normalized to the first EPSP in the recorded 20 or 50 Hz train from the same cell. We subsequently convolved the single EPSP waveform with a 20 or 50 Hz binary pulse train using the Matlab function convr(). We then calculated the peak amplitude ratios for each EPSP in observed and expected trains.

For the free-field sound presentation experiments of Figure 7D-E, we limited our analyses to superficial IC neurons that showed onset EPSPs in response to clicks. Other IC neurons encountered during these experiments showed either sound-evoked IPSPs (n=7 cells from N=5 mice) or IPSPs followed by rebound depolarizations (n=6 cells from N=5 mice); analyses of these data will be presented in a separate report.

In dual pathway experiments of Figure 8, the onset latency of ascending and descending EPSPs varied across cells. Thus, the relative timing of electrical and optogenetic stimulation during combined pathway activation was calculated online and on a cell-by-cell basis, such that the onset of descending auditory cortical EPSPs collided with the peak of ascending EPSPs from central IC as predicted from our *in vivo* latency measurements (Figure 7; range of Δt between stimulation of descending and ascending synapses: -1.3 to 16.4 ms). These stimulation parameters were held constant across control and R-CPP conditions for each cell. The expected linear summation was calculated by digitally summing the average synaptic waveforms following stimulation of either pathway alone, accounting for the temporal offset employed during synchronous pathway activation.

Histology and Confocal Imaging: Mice were deeply anesthetized in a glass induction chamber circulated with 4.2 mL isoflurane and transcardially perfused with ~80-100 mL of PBS followed by ~80-100 mL of 10% buffered formalin (Fisher Scientific catalog # 23-245684). Brains were carefully removed, stored in 10% formalin and protected from light for 24 hours. Subsequently, brains were stored in PBS for up to 72 hours and 100 µm thick coronal slices were cut using a ceramic blade (Cadence Endurium) and a Leica VT1000s vibratome, mounted onto slides and coverslipped using Fluoromount, then protected from light and allowed to dry at room temperature for ~12-24 hours.

Slides were then stored at 4 C until ready for use. Images were collected using a Leica TCS SP8 laser scanning confocal microscope equipped with a 10x objective.

Statistics: Although not explicitly pre-determined prior to data collection, sample sizes reflect commonly accepted standards in the field. Data were tested for normality using a Lilliefors test prior to statistical comparisons. Parametric, two-tailed t-tests are employed for normally distributed data. Non-parametric rank-sum or sign-rank tests are used when one or more of the distributions deviate from normal. Alpha is corrected for multiple comparisons in post-hoc significance tests following ANOVA. Statistics were run in Matlab or Graphpad Prism 9.

Author Contributions: HMO conducted and analyzed most electrophysiology experiments in Figure 7, with contributions from PFA. HMO, AF, and JC performed viral injections. AF performed histology and confocal microscopy experiments in Figure 1. PFA conducted and analyzed most electrophysiology experiments in Figures 1-6 and Figure 8, with contributions from HMO. PFA designed the experiments, interpreted the results, and wrote the paper.

Acknowledgments: Funding was generously provided by the Whitehall Foundation, Hearing Health Foundation, and NIH/NIDCD R01DC019090 to PFA, as well as T32 DC005356 and T32 DC000011 pre-doctoral awards to HMO. We thank Mr. Deepak Dileepkumar for outstanding technical support, Drs. Michael Roberts, Marina Silveira, Gunnar Quass and Meike Rogalla for critical comments on the manuscript.

References

Abbott LF, Varela JA, Sen K, Nelson SB (1997) Synaptic depression and cortical gain control. Science 275:220–224.

Ahuja TK, Wu SH (2007) Intrinsic membrane properties and synaptic response characteristics of neurons in the rat's external cortex of the inferior colliculus. Neuroscience 145:851–865.

Anderson LA, Malmierca MS (2013) The effect of auditory cortex deactivation on stimulus-specific adaptation in the inferior colliculus of the rat. Eur J Neurosci 37:52–62.

Arnth-Jensen N, Jabaudon D, Scanziani M (2002) Cooperation between independent hippocampal synapses is controlled by glutamate uptake. Nat Neurosci 5:325–331.

Ayala YA, Udeh A, Dutta K, Bishop D, Malmierca MS, Oliver DL (2015) Differences in the strength of cortical and brainstem inputs to SSA and non-SSA neurons in the inferior colliculus. Sci Rep 5:10383.

Bajo VM, Nodal FR, Korn C, Constantinescu AO, Mann EO, Boyden ES, King AJ (2019) Silencing cortical activity during sound-localization training impairs auditory perceptual learning. Nat Commun 10:3075.

Bajo VM, Nodal FR, Moore DR, King AJ (2010) The descending corticocollicular pathway mediates learning-induced auditory plasticity. Nat Neurosci 13:253–260.

Barnstedt O, Keating P, Weissenberger Y, King AJ, Dahmen JC (2015) Functional Microarchitecture of the Mouse Dorsal Inferior Colliculus Revealed through In Vivo Two-Photon Calcium Imaging. J Neurosci 35:10927–10939.

Blackwell JM, Lesicko AM, Rao W, De Biasi M, Geffen MN (2020) Auditory cortex shapes sound responses in the inferior colliculus. eLife 9:e51890.

635 Bordi F, LeDoux JE (1994) Response properties of single units in areas of rat auditory thalamus that project to the
636 amygdala: II. Cells receiving convergent auditory and somatosensory inputs and cells antidromically activated
637 by amygdala stimulation. Exp Brain Res 98:275–286.

638 Brainard MS, Knudsen EI (1993) Experience-dependent plasticity in the inferior colliculus: a site for visual calibration of
639 the neural representation of auditory space in the barn owl. J Neurosci Off J Soc Neurosci 13:4589–4608.

640 Branco T, Clark BA, Häusser M (2010) Dendritic discrimination of temporal input sequences in cortical neurons.
641 Science 329:1671–1675.

642 Brown SP, Hestrin S (2009) Intracortical circuits of pyramidal neurons reflect their long-range axonal targets. Nature
643 457:1133–1136.

644 Cai D, Yue Y, Su X, Liu M, Wang Y, You L, Xie F, Deng F, Chen F, Luo M, Yuan K (2019) Distinct Anatomical
645 Connectivity Patterns Differentiate Subdivisions of the Nonlemniscal Auditory Thalamus in Mice. Cereb Cortex
646 29:2437–2454.

647 Champoux F, Paiement P, Mercier C, Lepore F, Lassonde M, Gagné J-P (2007) Auditory processing in a patient with a
648 unilateral lesion of the inferior colliculus: Role of the inferior colliculus in humans. Eur J Neurosci 25:291–297.

649 Chen C, Cheng M, Ito T, Song S (2018) Neuronal Organization in the Inferior Colliculus Revisited with Cell-Type-
650 Dependent Monosynaptic Tracing. J Neurosci 38:3318–3332.

651 Clements JD, Lester RA, Tong G, Jahr CE, Westbrook GL (1992) The time course of glutamate in the synaptic cleft.
652 Science 258:1498–1501.

653 Coomes DL, Schofield BR (2004) Projections from the auditory cortex to the superior olivary complex in guinea pigs.
654 Eur J Neurosci 19:2188–2200.

655 Destexhe A, Rudolph M, Paré D (2003) The high-conductance state of neocortical neurons in vivo. Nat Rev Neurosci
656 4:739–751.

657 Diamond IT, Jones EG, Powell TPS (1969) The projection of the auditory cortex upon the diencephalon and brain stem
658 in the cat. Brain Res 15:305–340.

659 Doucet JR, Molavi DL, Ryugo DK (2003) The source of corticocollicular and corticobulbar projections in area Te1 of the
660 rat. Exp Brain Res 153:461–466.

661 Faye-Lund H, Osen KK (1985) Anatomy of the inferior colliculus in rat. Anat Embryol (Berl) 171:1–20.

662 Feldman DE, Brainard MS, Knudsen EI (1996) Newly learned auditory responses mediated by NMDA receptors in the
663 owl inferior colliculus. Science 271:525–528.

664 Gasparini S, Magee JC (2006) State-dependent dendritic computation in hippocampal CA1 pyramidal neurons. J
665 Neurosci Off J Soc Neurosci 26:2088–2100.

666 Geis H-RAP, van der Heijden M, Borst JGG (2011) Subcortical input heterogeneity in the mouse inferior colliculus. J
667 Physiol 589:3955–3967.

668 Gottlieb Y, Vaadia E, Abeles M (1989) Single unit activity in the auditory cortex of a monkey performing a short term
669 memory task. Exp Brain Res 74:139–148.

670 Goyer D, Silveira MA, George AP, Beebe NL, Edelbrock RM, Malinski PT, Schofield BR, Roberts MT (2019) A novel
671 class of inferior colliculus principal neurons labeled in vasoactive intestinal peptide-Cre mice. eLife 8:e43770.

672 Harnett MT, Makara JK, Spruston N, Kath WL, Magee JC (2012) Synaptic amplification by dendritic spines enhances
673 input cooperativity. Nature 491:599–602.

674 Huang Y, Matysiak A, Heil P, König R, Brosch M (2016) Persistent neural activity in auditory cortex is related to
675 auditory working memory in humans and nonhuman primates. eLife 5.

676 Hurley LM, Pollak GD (2005) Serotonin shifts first-spike latencies of inferior colliculus neurons. J Neurosci Off J Soc
677 Neurosci 25:7876–7886.

678 Joswig H, Schönenberger U, Brügge D, Richter H, Surbeck W (2015) Reversible pure word deafness due to inferior
679 colliculi compression by a pineal germinoma in a young adult. Clin Neurol Neurosurg 139:62–65.

680 Kerchner GA, Nicoll RA (2008) Silent synapses and the emergence of a postsynaptic mechanism for LTP. Nat Rev
681 Neurosci 9:813–825.

682 Kitagawa M, Sakaba T (2019) Developmental changes in the excitatory short-term plasticity at input synapses in the rat
683 inferior colliculus. Eur J Neurosci 50:2830–2846.

684 Kole MHP, Letzkus JJ, Stuart GJ (2007) Axon initial segment Kv1 channels control axonal action potential waveform
685 and synaptic efficacy. Neuron 55:633–647.

686 Kong L, Xiong C, Li L, Yan J (2014) Frequency-specific corticofugal modulation of the dorsal cochlear nucleus in mice.
687 Front Syst Neurosci 8 Available at: http://journal.frontiersin.org/article/10.3389/fnsys.2014.00125/abstract
688 [Accessed November 16, 2020].

689 Krishna BS, Semple MN (2000) Auditory Temporal Processing: Responses to Sinusoidally Amplitude-Modulated Tones
690 in the Inferior Colliculus. J Neurophysiol 84:255–273.

691 Larkum ME, Nevian T, Sandler M, Polsky A, Schiller J (2009) Synaptic Integration in Tuft Dendrites of Layer 5
692 Pyramidal Neurons: A New Unifying Principle. Science 325:756–760.

693 LeDoux J, Farb C, Ruggiero D (1990) Topographic organization of neurons in the acoustic thalamus that project to the
694 amygdala. J Neurosci 10:1043–1054.

695 Lefort S, Tomm C, Floyd Sarria J-C, Petersen CCH (2009) The excitatory neuronal network of the C2 barrel column in
696 mouse primary somatosensory cortex. Neuron 61:301–316.

697 Lesicko AMH, Hristova TS, Maigler KC, Llano DA (2016) Connectional Modularity of Top-Down and Bottom-Up
698 Multimodal Inputs to the Lateral Cortex of the Mouse Inferior Colliculus. J Neurosci 36:11037–11050.

699 Lester RA, Jahr CE (1992) NMDA channel behavior depends on agonist affinity. J Neurosci Off J Soc Neurosci
700 12:635–643.

701 Li Y, Evans MS, Faingold CL (1998) In vitro electrophysiology of neurons in subnuclei of rat inferior colliculus. Hear Res
702 121:1–10.

703 Llano DA, Slater BJ, Lesicko AMH, Stebbings KA (2014) An auditory colliculothalamocortical brain slice preparation in
704 mouse. J Neurophysiol 111:197–207.

705 Loftus WC, Malmierca MS, Bishop DC, Oliver DL (2008) The cytoarchitecture of the inferior colliculus revisited: A
706 common organization of the lateral cortex in rat and cat. Neuroscience 154:196–205.

707 Losonczy A, Magee JC (2006) Integrative properties of radial oblique dendrites in hippocampal CA1 pyramidal
708 neurons. Neuron 50:291–307.

709 Lumani A, Zhang H (2010) Responses of neurons in the rat's dorsal cortex of the inferior colliculus to monaural tone
710 bursts. Brain Res 1351:115–129.

711 Ma CL, Kelly JB, Wu SH (2002) AMPA and NMDA receptors mediate synaptic excitation in the rat's inferior colliculus.
712 Hear Res 168:25–34.

713 Markram H, Wang Y, Tsodyks M (1998) Differential signaling via the same axon of neocortical pyramidal neurons. Proc
714 Natl Acad Sci U S A 95:5323–5328.

715 Massopust LC, Ordy JM (1962) Auditory organization of the inferior colliculi in the cat. Exp Neurol 6:465–477.

716 Masterton RB, Jane JA, Diamond IT (1968) Role of brain-stem auditory structures in sound localization. II. Inferior
717 colliculus and its brachium. J Neurophysiol 31:96–108.

718 Mellott JG, Foster NL, Ohl AP, Schofield BR (2014) Excitatory and inhibitory projections in parallel pathways from the
719 inferior colliculus to the auditory thalamus. Front Neuroanat 8 Available at:
720 http://journal.frontiersin.org/article/10.3389/fnana.2014.00124/abstract [Accessed July 24, 2020].

721 Mitani A, Shimokouchi M, Nomura S (1983) Effects of stimulation of the primary auditory cortex upon
722 colliculogeniculate neurons in the inferior colliculus of the cat. Neurosci Lett 42:185–189.

723 Moore LA, Trussell LO (2017) Corelease of Inhibitory Neurotransmitters in the Mouse Auditory Midbrain. J Neurosci Off
724 J Soc Neurosci 37:9453–9464.

725 Morris RG, Anderson E, Lynch GS, Baudry M (1986) Selective impairment of learning and blockade of long-term
726 potentiation by an N-methyl-D-aspartate receptor antagonist, AP5. Nature 319:774–776.

727 Nakamoto KT, Jones SJ, Palmer AR (2008) Descending projections from auditory cortex modulate sensitivity in the
728 midbrain to cues for spatial position. J Neurophysiol 99:2347–2356.

729 Nakamoto KT, Shackleton TM, Palmer AR (2010) Responses in the inferior colliculus of the guinea pig to concurrent
730 harmonic series and the effect of inactivation of descending controls. J Neurophysiol 103:2050–2061.

731 Naumov V, Heyd J, de Arnal F, Koch U (2019) Analysis of excitatory and inhibitory neuron types in the inferior
732 colliculus based on I_h properties. J Neurophysiol 121:2126–2139.

733 Oliver DL (1984) Neuron types in the central nucleus of the inferior colliculus that project to the medial geniculate body.
734 Neuroscience 11:409–424.

735 Oliver DL, Hall WC (1978) The medial geniculate body of the tree shrew,Tupaia glis I. Cytoarchitecture and midbrain
736 connections. J Comp Neurol 182:423–458.

737 Peña JL, Konishi M (2001) Auditory spatial receptive fields created by multiplication. Science 292:249–252.

738 Pena JL, Konishi M (2002) From postsynaptic potentials to spikes in the genesis of auditory spatial receptive fields. J
739 Neurosci Off J Soc Neurosci 22:5652–5658.

740 Peruzzi D, Sivaramakrishnan S, Oliver DL (2000) Identification of cell types in brain slices of the inferior colliculus.
741 Neuroscience 101:403–416.

742 Polsky A, Mel B, Schiller J (2009) Encoding and decoding bursts by NMDA spikes in basal dendrites of layer 5
743 pyramidal neurons. J Neurosci Off J Soc Neurosci 29:11891–11903.

744 Ponvert ND, Jaramillo S (2019) Auditory Thalamostriatal and Corticostriatal Pathways Convey Complementary
745 Information about Sound Features. J Neurosci 39:271–280.

746 Pouille F, Scanziani M (2004) Routing of spike series by dynamic circuits in the hippocampus. Nature 429:717–723.

747 Qi J, Zhang Z, He N, Liu X, Zhang C, Yan J (2020) Cortical Stimulation Induces Excitatory Postsynaptic Potentials of
748 Inferior Colliculus Neurons in a Frequency-Specific Manner. Front Neural Circuits 14:591986.

749 Ranganathan GN, Apostolides PF, Harnett MT, Xu N-L, Druckmann S, Magee JC (2018) Active dendritic integration
750 and mixed neocortical network representations during an adaptive sensing behavior. Nat Neurosci 21:1583–
751 1590.

752 Ruediger S, Scanziani M (2020) Learning speed and detection sensitivity controlled by distinct cortico-fugal neurons in
753 visual cortex. eLife 9.

754 Ryugo DK, Weinberger NM (1976) Corticofugal modulation of the medial geniculate body. Exp Neurol 51:377–391.

Sakurai Y (1990) Cells in the rat auditory system have sensory-delay correlates during the performance of an auditory working memory task. Behav Neurosci 104:856–868.

Saldaña E, Feliciano M, Mugnaini E (1996) Distribution of descending projections from primary auditory neocortex to inferior colliculus mimics the topography of intracollicular projections. J Comp Neurol 371:15–40.

Saldaña E, Merchán MA (1992) Intrinsic and commissural connections of the rat inferior colliculus. J Comp Neurol 319:417–437.

Schofield BR, Coomes DL, Schofield RM (2006) Cells in Auditory Cortex that Project to the Cochlear Nucleus in Guinea Pigs. J Assoc Res Otolaryngol 7:95–109.

Schwartz EJ, Rothman JS, Dugué GP, Diana M, Rousseau C, Silver RA, Dieudonné S (2012) NMDA receptors with incomplete Mg^{2+} block enable low-frequency transmission through the cerebellar cortex. J Neurosci Off J Soc Neurosci 32:6878–6893.

Silveira MA, Anair JD, Beebe NL, Mirjalili P, Schofield BR, Roberts MT (2020) Neuropeptide Y Expression Defines a Novel Class of GABAergic Projection Neuron in the Inferior Colliculus. J Neurosci 40:4685–4699.

Sinex DG, Li H (2007) Responses of Inferior Colliculus Neurons to Double Harmonic Tones. J Neurophysiol 98:3171–3184.

Sivaramakrishnan S, Oliver DL (2001) Distinct K currents result in physiologically distinct cell types in the inferior colliculus of the rat. J Neurosci Off J Soc Neurosci 21:2861–2877.

Smith PH (1992) Anatomy and physiology of multipolar cells in the rat inferior collicular cortex using the in vitro brain slice technique. J Neurosci Off J Soc Neurosci 12:3700–3715.

Song JH, Lucaci D, Calangiu I, Brown MTC, Park JS, Kim J, Brickley SG, Chadderton P (2018) Combining mGRASP and Optogenetics Enables High-Resolution Functional Mapping of Descending Cortical Projections. Cell Rep 24:1071–1080.

Stebbings KA, Lesicko AMH, Llano DA (2014) The auditory corticocollicular system: Molecular and circuit-level considerations. Hear Res 314:51–59.

Stuart GJ, Spruston N (2015) Dendritic integration: 60 years of progress. Nat Neurosci 18:1713–1721.

Sun H, Wu SH (2008) Modification of membrane excitability of neurons in the rat's dorsal cortex of the inferior colliculus by preceding hyperpolarization. Neuroscience 154:257–272.

Sun H, Wu SH (2009) The physiological role of pre- and postsynaptic GABA(B) receptors in membrane excitability and synaptic transmission of neurons in the rat's dorsal cortex of the inferior colliculus. Neuroscience 160:198–211.

Suthakar K, Ryugo DK (2017) Descending projections from the inferior colliculus to medial olivocochlear efferents: Mice with normal hearing, early onset hearing loss, and congenital deafness. Hear Res 343:34–49.

Syka J, Popelár J, Kvasnák E, Astl J (2000) Response properties of neurons in the central nucleus and external and dorsal cortices of the inferior colliculus in guinea pig. Exp Brain Res 133:254–266.

Takahashi H, Magee JC (2009) Pathway interactions and synaptic plasticity in the dendritic tuft regions of CA1 pyramidal neurons. Neuron 62:102–111.

Vila C-H, Williamson RS, Hancock KE, Polley DB (2019) Optimizing optogenetic stimulation protocols in auditory corticofugal neurons based on closed-loop spike feedback. J Neural Eng 16:066023.

Weible AP, Yavorska I, Wehr M (2020) A Cortico-Collicular Amplification Mechanism for Gap Detection. Cereb Cortex N Y N 1991 30:3590–3607.

Williamson RS, Polley DB (2019) Parallel pathways for sound processing and functional connectivity among layer 5 and 6 auditory corticofugal neurons. eLife 8:e42974.

796 Winer JA (2006) Decoding the auditory corticofugal systems. Hear Res 212:1–8.

797 Winer JA, Diehl JJ, Larue DT (2001) Projections of auditory cortex to the medial geniculate body of the cat. J Comp
798 Neurol 430:27–55.

799 Winer JA, Larue DT, Diehl JJ, Hefti BJ (1998) Auditory cortical projections to the cat inferior colliculus. J Comp Neurol
800 400:147–174.

801 Wong AB, Borst JGG (2019) Tonotopic and non-auditory organization of the mouse dorsal inferior colliculus revealed
802 by two-photon imaging. eLife 8:e49091.

803 Wu SH (2004) Contribution of AMPA, NMDA, and GABAA Receptors to Temporal Pattern of Postsynaptic Responses
804 in the Inferior Colliculus of the Rat. J Neurosci 24:4625–4634.

805 Xiao Z, Suga N (2002) Modulation of cochlear hair cells by the auditory cortex in the mustached bat. Nat Neurosci
806 5:57–63.

807 Xiong XR, Liang F, Zingg B, Ji X, Ibrahim LA, Tao HW, Zhang LI (2015) Auditory cortex controls sound-driven innate
808 defense behaviour through corticofugal projections to inferior colliculus. Nat Commun 6:7224.

809 Yan J, Suga N (1999) Corticofugal Amplification of Facilitative Auditory Responses of Subcortical Combination-
810 Sensitive Neurons in the Mustached Bat. J Neurophysiol 81:817–824.

811 Yan W, Suga N (1998) Corticofugal modulation of the midbrain frequency map in the bat auditory system. Nat Neurosci
812 1:54–58.

813 Yu Y-Q, Xiong Y, Chan Y-S, He J (2004) Corticofugal gating of auditory information in the thalamus: an in vivo
814 intracellular recording study. J Neurosci Off J Soc Neurosci 24:3060–3069.

815 Zucker RS, Regehr WG (2002) Short-term synaptic plasticity. Annu Rev Physiol 64:355–405.

816

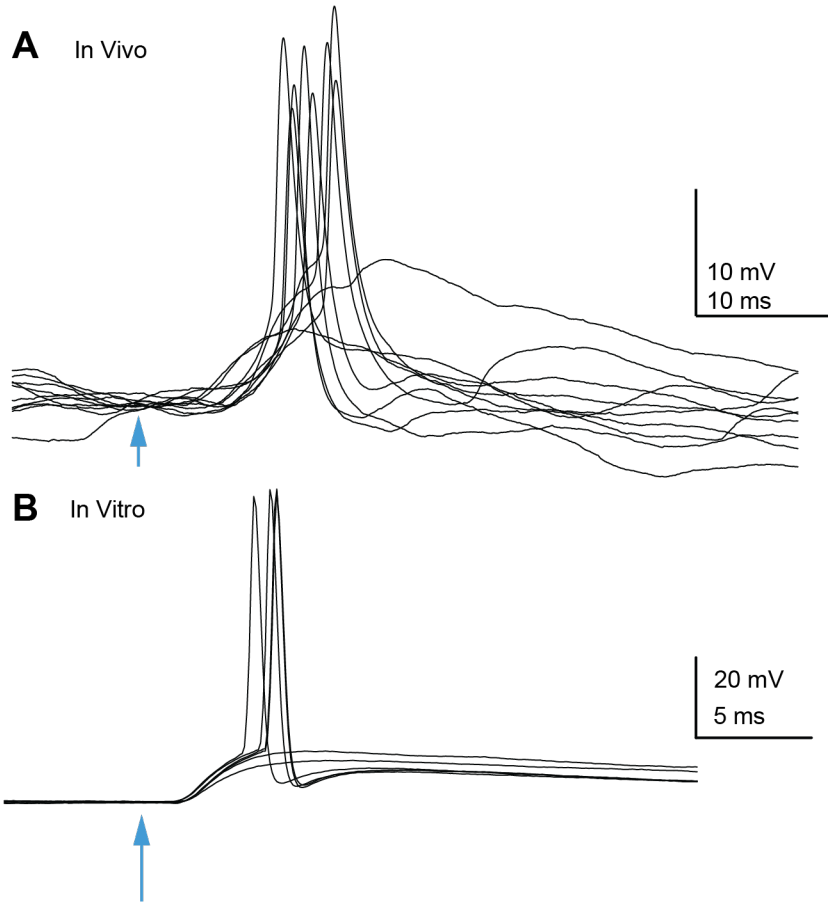

Supplemental Figure 1: *Auditory cortico-collicular EPSPs can trigger spikes in IC neurons in vivo and in vitro.*
A) Example overlaid trials from an *in vivo* whole-cell recording of a superficial IC neuron. Optogenetic stimulation of auditory cortex denoted by arrowhead.
B) Example trials from an *in vitro* recording.

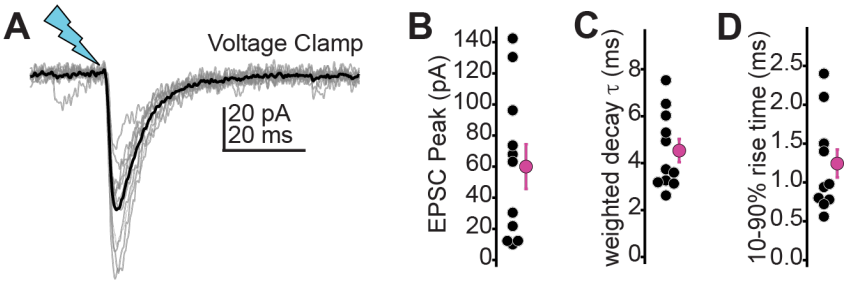

822 Supplemental Figure 2: *Auditory Cortico-collicular transmission in voltage-clamp.*
823 **A)** Example EPSCs recorded in voltage clamp. Gray and black traces are individual trials and
824 average, respectively. **B-D)** Summary data for EPSC peak amplitudes (B), decay time constant (C),
825 and 10-90% rise time (D) in n=11 cells.

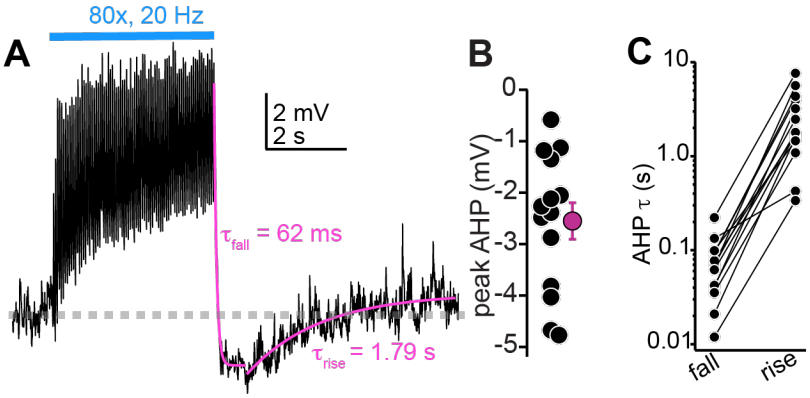

826 Supplemental Figure 3: *Large AHPs follow the cessation of auditory cortico-collicular activity in*
827 *vivo.*
828 **A)** Membrane potential (average of multiple trials) during prolonged auditory cortical activity *in vivo*.
829 Magenta are mono-exponential fits to the membrane potential fall and rise upon cessation of
830 optogenetic stimulation.
831 **B)** Peak AHP amplitude (relative to baseline Vm) in n=14 cells.
832 **C)** Time constants for the fall and raise of the membrane potential for n = 14 cells. The data are on
833 a log scale due to the order of magnitude difference in exponent values for fall and rise.

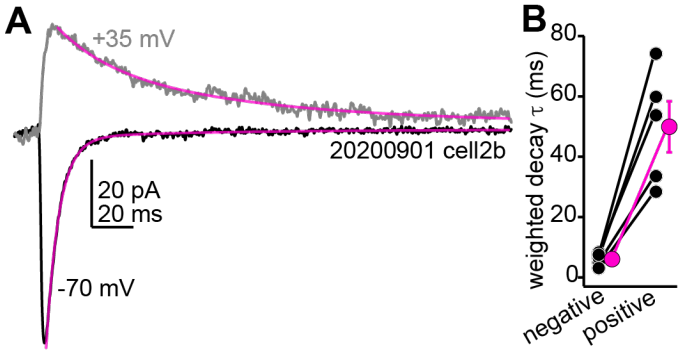

834 Supplemental Figure 4: *Auditory cortico-collicular EPSCs recorded at positive potentials are slower*
835 *than at negative potentials, consistent with the presence of NMDA receptors.*
836 **A)** Example average EPSCs recorded at negative and positive potentials. Magenta are double
837 exponential fits to the EPSC decay.
838 **B)** Decay time constant for n=5 cells recorded at positive and negative voltages.